Commun Nonlinear Sci Numer Simulat 17 (2012) 2021–2030

Contents lists available at ScienceDirect

Commun Nonlinear Sci Numer Simulat

journal homepage: www.elsevier.com/locate/cnsns

Nontwist symplectic maps in tokamaks

I.L. Caldas [a], R.L. Viana [b,*], J.D. Szezech Jr. [a], J.S.E. Portela [a], J. Fonseca [a], M. Roberto [c], C.G.L. Martins [c], E.J. da Silva [a]

[a] Instituto de Física, Universidade de São Paulo, 05315-970 São Paulo, Brazil
[b] Departamento de Física, Universidade Federal do Paraná, 81531-990 Curitiba, Paraná, Brazil
[c] Instituto Tecnológico de Aeronáutica, São José dos Campos, São Paulo, Brazil

ARTICLE INFO

Article history:
Available online 6 June 2011

Dedicated to Prof. Phil Morrison on occasion of his 60th birthday.

Keywords:
Symplectic maps
Nontwist systems
Tokamaks

ABSTRACT

We review symplectic nontwist maps that we have introduced to describe Lagrangian transport properties in magnetically confined plasmas in tokamaks. These nontwist maps are suitable to describe the formation and destruction of transport barriers in the shearless region (i.e., near the curve where the twist condition does not hold). The maps can be used to investigate two kinds of problems in plasmas with non-monotonic field profiles: the first is the chaotic magnetic field line transport in plasmas with external resonant perturbations. The second problem is the chaotic particle drift motion caused by electrostatic drift waves. The presented analytical maps, derived from plasma models with equilibrium field profiles and control parameters that are commonly measured in plasma discharges, can be used to investigate long-term transport properties.

1. Introduction

Symplectic maps have been for a long time used as models of Hamiltonian systems [1]. Such maps may arise from intersections of phase space trajectories with a given surface of section, or also may appear as stroboscopic samplings of a trajectory of a time-dependent system at fixed time intervals [2]. If the time dependence is a periodic sequence of delta function kicks it is possible to obtain explicit formulas for the maps [1,3]. Symplectic maps are convenient systems to investigate, inasmuch we can compute a large number of iterations using a short CPU time and practically without propagating numerical errors. This is particularly important in investigations of Hamiltonian transport requiring computation of phase space trajectories during a very long time interval.

Traditionally studies of symplectic maps deal with twist maps for which the rotation number varies monotonically. Many important theoretical results, like Kolmogorov–Arnold–Moser (KAM) and Poincaré–Birkhoff theorems, and Aubry–Mather theory are stated for two-dimensional symplectic maps [2].

Recently there is a growing interest in nontwist maps, for which the twist condition is not fulfilled for all points in the domain of interest [2,4]. Nontwist maps are of mathematical interest because only a few rigorous results exist for them [5–9].

Moreover, nontwist maps also appear in many dynamical systems of physical interest, often related to continuous systems like fluids and plasmas, such as magnetic field lines in toroidal plasma devices with reversed magnetic shear [4,10–14], advection by incompressible shear flows [15], traveling waves in geophysical zonal flows [16,17], and the $\mathbf{E} \times \mathbf{B}$ drift motion of charged particles in a magnetized plasma under the action of a time-periodic electric field from an

* Corresponding author.
E-mail address: viana@fisica.ufpr.br (R.L. Viana).

1007-5704/$ - see front matter © 2011 Elsevier B.V. All rights reserved.
doi:10.1016/j.cnsns.2011.05.040

electrostatic wave [18–21]. Nontwist maps have also been investigated in particle motions described by certain Hamiltonians in molecular physics [22,23].

Here, we review examples of nontwist maps that we have proposed, some of them in collaboration with Phil Morrison. For magnetically confined plasmas in tokamaks, nontwist maps are introduced to describe the presence of Lagrangian chaos at the plasma edge. Initially we consider the Lagrangian description of magnetic field lines in tokamaks [10,21]. In this description the field lines for a confined plasma with a non-monotonic electric current density are mapped into a two-dimensional Poincaré surface of section with a nontwist rotation number radial profile. This nontwist condition at the plasma edge creates a barrier to the field line that attenuates the plasma transport, so improving plasma confinement [24].

In the second place we consider the chaotic motion of particles at the plasma edge in an equilibrium electric field with non-monotonic radial profile perturbed by drift waves [16,18,20]. For these profiles the particle trajectories can be also mapped in to a two-dimensional Poincaré section with a nontwist rotation number radial profile, a result similar to that obtained for magnetic field lines. To illustrate that we present a new nontwist drift map obtained for a nonmonotonic electric potential that creates a transport barrier in the nontwist region.

This paper is organized as follows: in Section 2 we introduce the symplectic nontwist maps through its most studied example, the standard nontwist map introduced by Phil Morrison and his collaborators. Sections 3 and 4 present, respectively, the nontwist maps we derived for magnetic field lines and particle transport in tokamaks. Our conclusions are left to the final Section.

2. Nontwist symplectic maps

Let (x_n,y_n) be the normalized angle and action variables, respectively, of a phase space trajectory at its nth piercing with a Poincaré surface of section, such that $y_n \in \mathbb{R}$ and $x_n \in (-1/2, 1/2]$. We will consider two-dimensional symplectic maps of the form

$$y_{n+1} = y_n + f(x_n), \tag{1}$$

$$x_{n+1} = x_n - g(y_{n+1}), \quad (mod 1) \tag{2}$$

where $f(x_n)$ is a period-1 function of its argument, standing for the perturbation strength. We assume that the time-dependence of the perturbing term can be modeled by a periodic delta function. Moreover $g(y_{n+1})$ is the winding number of the unperturbed trajectories, its derivative being the so-called shear function. If g is a monotonically increasing or decreasing function the corresponding shear does not change sign, giving the twist condition:

$$|g'(y_{n+1})| = \left|\frac{\partial x_{n+1}}{\partial y_n}\right| \geqslant c > 0, \tag{3}$$

where $c \in \mathbb{R}$.

However, for a non-monotonic g-profile the twist condition is not satisfied at some point y_s and $g'(y_s) = 0$ determines the shearless curve. If the winding number $g(y)$ has only one extremum at the shearless curve $y = y_S$, we can expand this function in the vicinity of this point. The lowest-order approximation for $g(y)$ is thus a quadratic function. On keeping one Fourier mode in the perturbation term of (1) and (2), we obtain the standard non-twist map (SNTM) [16]

$$x_{n+1} = x_n + a(1 - y_{n+1}^2), \tag{4}$$

$$y_{n+1} = y_n - b\sin(2\pi x_n), \tag{5}$$

where $a \in (0,1)$, and $b > 0$.

The mathematical properties of SNTM have been extensively investigated by Phil Morrison and his collaborators over the past two decades [25]. In the following we outline some of these properties, referring to the literature for a more complete coverage of them. In the unperturbed case ($b = 0$) the twist condition (3) is violated at the point $y_S = 0$, what defines a shearless curve $\{y = y_S = 0\}$. The quadratic form of g around $y_S = 0$ leads to two invariant curves located at $y = \pm y_0$ and with the same winding number $a(1 - y_0^2)$ at both sides of the shearless curve.

As the perturbation becomes nonzero ($b \neq 0$) two periodic island chains appear at the two invariant curve locations, and the former shearless curve becomes a shearless invariant tori separating these two island chains [16]. There are also chaotic layers attached to the "separatrices" of both island chains, as expected from the presence of homoclinic crossings therein. These chaotic layers are not connected, though, as far as there are invariant curves near the shearless invariant tori acting as dikes, preventing global transport [26].

A representative example of this scenario is provided by Fig. 1(a), where a phase portrait of the SNTM is depicted for $b = 0.410$ and $a = 0.700$. We observe two island chains with three islands each and the same winding number. The local maxima of the perturbed winding number profile define a shearless invariant curve, which existence can be inferred between the two island chains. The island chains bordering the shearless invariant curve are transport barriers, since chaotic trajectories above and below do not mix. If, however, the parameters are further modified, another noteworthy feature of nontwist maps can emerge, depending on the parameter space region. In one scenario (generic reconnection) the island chains with the same winding number approach each other and their unstable and stable invariant manifolds suffer a (non-dissipative)

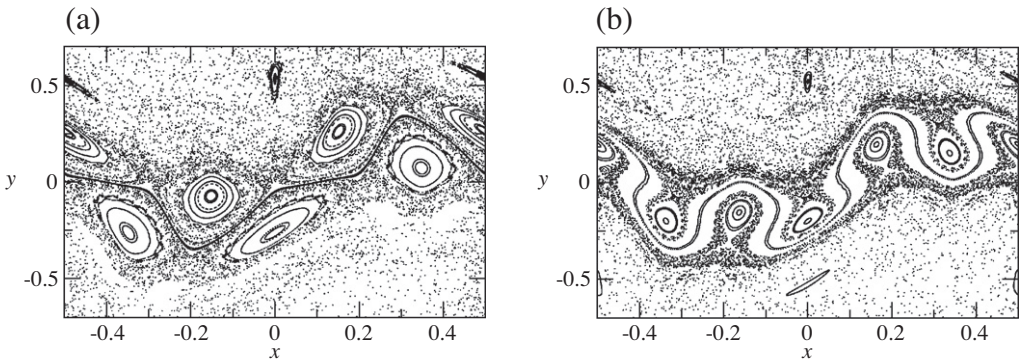

Fig. 1. Phase portrait of the standard non-twist map (4) and (5) for $b = 0.410$ and (a) $a = 0.700$; (b) $a = 0.690$.

reconnection. The latter can be recognized in Fig. 1(b), the phase portrait obtained for the same value of the parameter b of Fig. 1(a) but changing the parameter a to 0.690.

In the region between the chains, there appear new invariant tori called meandering curves (which are not KAM tori, though, since the latter must be a graph over x, while meanders are not). The remaining periodic orbits eventually coalesce and disappear, leaving only meanders and the shearless torus. This set of curves turns out to be a robust transport barrier, as illustrated by Fig. 2(a), where three chaotic orbits at different sides of the barrier are kept segregated by a shearless curve [27]. The other possible reconnection scenario, described in Ref. [28] is non-generic and involves the formation of vortex pairs, that is possible only in nontwist maps with certain symmetries. Further growth of b-parameter causes the breakup of the transport barrier and the consequent mixing of the chaotic orbits formerly segregated at both sides of the shearless invariant torus Fig. 2(b).

3. Magnetic field line maps in tokamaks

In the program to develop controlled thermonuclear fusion, tokamaks have been used to carry out experiments with magnetically confined plasmas. In the last years it became evident that the plasma confinement strongly depends on the confining magnetic field spatial profiles at the plasma edge [29]. The influence of these fields on the plasma-wall interactions, the plasma edge electrostatic turbulence, and the anomalous particle transport induced by this turbulence are nowadays under intense investigation in all tokamaks [30]. In tokamaks, the magnetic field at the plasma edge is made chaotic to control the ELM instability [31] and to smear out large heat and particle loads on the wall [32]. However, in the chaotic field region the

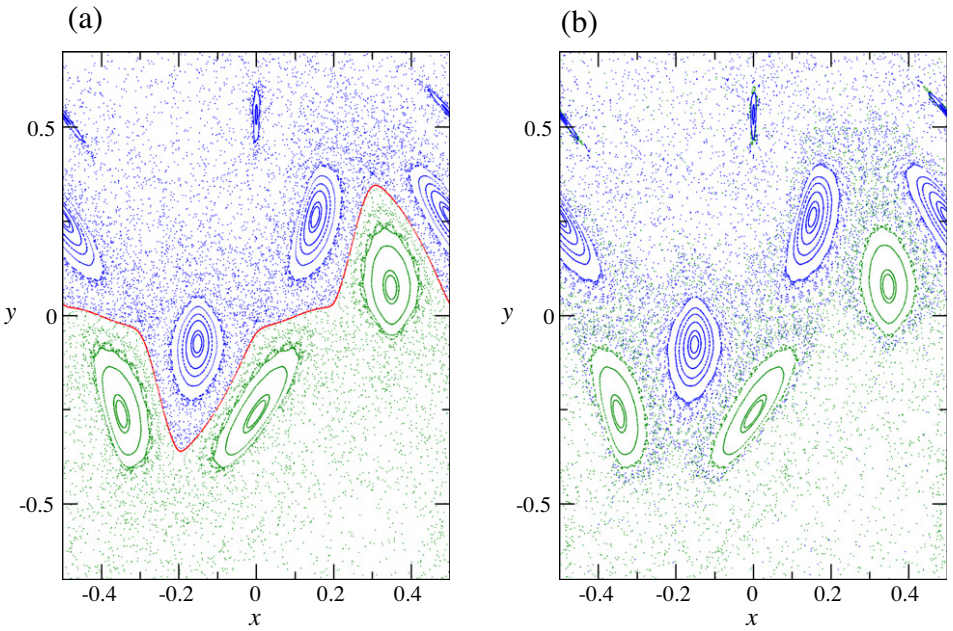

Fig. 2. Phase portrait of the standard non-twist map (4) and (5) for $a = 0.700$ and (a) $b = 0.412$; (b) $b = 0.414$.

lines escape to the wall through a fractal like structure and, for some discharge parameters, the line escape gives rise to a footprint with high concentration of heat and particle loadings on the tokamak wall [31,32].

Before presenting tokamak maps which have been constructed to evidence the above-mentioned effects, let us describe very briefly the tokamak geometry and how the magnetic field lines are characterized. The tokamak is a toroidal vessel with major radius R_0 and minor radius b, its aspect ratio being b/R_0. The major radius defines a magnetic axis, with respect to which a field line is described using three "local" coordinates: a radius r, a poloidal angle θ and a toroidal angle φ [29]. A Poincaré surface of section is a plane where φ is a constant, intersecting the field line at a point with coordinates (r_n, θ_n), n being an integer. Actually, (r_n, θ_n) are not canonical coordinates themselves, but we can construct such an action-angle pair, depending on the specific case. Nevertheless the field line maps so obtained are symplectic thanks to the solenoidal condition $\nabla \cdot \mathbf{B} = 0$ [29].

The equilibrium magnetic field in a tokamak leads to helical magnetic fields lying on nested tori concentric with the magnetic axis. Each torus can be characterized by its safety factor $q(r,\theta) = d\varphi/d\theta$. If q is a rational (irrational) number the corresponding torus is likewise rational (irrational)[29]. Nontwist maps arise from non-monotonic safety factors, as we shall see.

3.1. Ullmann map

If the aspect ratio is large, we can use a periodic cylinder approximation and add toroidicity effects later on as a perturbing term. In this spirit the Ullmann map (UM) [24] models the magnetic fields in a tokamak with an ergodic limiter [33–35]. It can be obtained from a second kind generating function and was inspired by an earlier model [37]. The UM satisfies the conditions for a tokamak model outlined in [36], further including toroidal effects and presenting the advantage of having its parameters directly related to experimental ones.

The UM is given as a composition of two maps:the equilibrium map

$$r_{n+1} = \frac{r_n}{1 - a_1 \sin\theta_n}, \tag{6}$$

$$\theta_{n+1} = \theta_n + \frac{2\pi}{q_{\mathrm{eq}}(r_{n+1})} + a_1 \cos\theta_n \ (\mathrm{mod}\ 2\pi), \tag{7}$$

and the perturbation map

$$r_n = r_{n+1} + \frac{mC\epsilon b}{m-1}\left(\frac{r_{n+1}}{b}\right)^{m-1} \sin(m\theta_n), \tag{8}$$

$$\theta_{n+1} = \theta_n - C\epsilon\left(\frac{r_{n+1}}{b}\right)^{m-2} \cos(m\theta_n), \tag{9}$$

where the parameter a_1 gives the strength of the toroidal correction in the cylindrical equilibrium, and ϵ is proportional to the current in the limiter, quantifying the perturbation strength due to the magnetic ergodic limiter (m and C are geometrical factors) [37].

The freely adjustable equilibrium safety factor profile $q_{\mathrm{eq}}(r)$ appearing in Eq. (7) is an additional advantage of the UM and the following expression describes in a satisfactory way typical non-monotonic q-profiles for plasma discharges in tokamak experiments [24]

$$q(r) = q_a \frac{r^2}{a^2}\left[1 - \left(1 + \beta'\frac{r^2}{a^2}\right)\left(1 - \frac{r^2}{a^2}\right)^{\mu+1} \Theta(a-r)\right]^{-1}, \tag{10}$$

where a is the plasma radius; q_a, γ, β, and μ are parameters that can be chosen to fit experimentally observed plasma profiles ($\beta' = \beta(\mu+1)/(\beta+\mu+1)$), and Θ is the unit step function. With this profile the UM becomes a nontwist one.

Giving that the UM is intended to study the tokamak edge, r and θ being planar coordinates in the rectangular approximation, it is convenient to consider normalized coordinates: $y = 1 - r/b$ and $x = \theta/2\pi$, so that the tokamak wall lies at $y = 0$. In Fig. 3 we show phase portraits for UM, highlighting the invariant curves [depicted in red[1]) between the island chains involved in the reconnection scenario typical of nontwist maps. In Fig. 3(a) we have two island chains separated by invariant curves, whereas in Fig. 3(b) there occurs a heteroclinic connection. After a further increase of the perturbation the hyperbolic (saddle) points of the island chains interchanged Fig. 3(c). Even after an island chain disappears through a saddle-center bifurcation, the transport barrier still persists [depicted in red in Fig. 3(d)].

It is worth considering the detailed structure of the region near the shearless curve before and after the transport barrier has been destructed. Fig. 4(a) shows a magnification of the barrier region depicting in red the island chains inside the barrier. The region around the islands left after the destruction of the barrier is shown in Fig. 4(b). The concentration of orbit points in this region characterizes the stickness phenomenon, which is the tendency of chaotic orbits near the remaining island to stay there for a long time before being returning to the chaotic sea. These sticky regions exert a strong influence on the transport properties of Hamiltonian systems, since they act as dynamical traps, in such a way that the transport becomes anomalous.

[1] For interpretation of colour in Figs. 3 and 4, the reader is referred to the web version of this article.

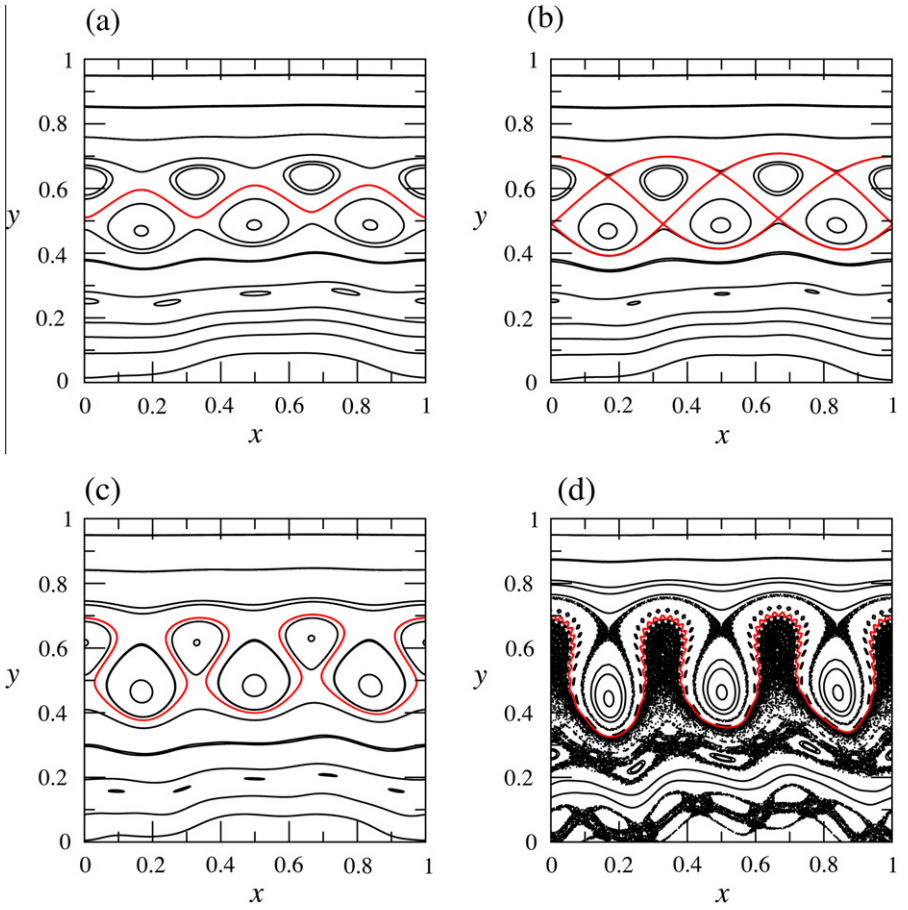

Fig. 3. Phase portraits for UM for (a) $\epsilon = 0.05$; (b) $\epsilon = 0.0635$; (c) $\epsilon = 0.10$; (d) $\epsilon = 0.30$.

In Fig. 5(a) we display a magnification of the effective barrier region showing different regions in the chaotic sea separated by broken invariant lines, the cantori, just after the invariant barrier destruction. For a slightly higher perturbation value, [Fig. 5(b)] this region acts less like a barrier to the transport.

3.2. Two-mode map

In the UM the dynamical variables are the coordinates (r,θ) of the intersection of a magnetic field line with a Poincaré surface. This rather simplified description has two problems: (i) the toroidicity effect is treated phenomenologically, i.e. it does not come from first principles; (ii) the variables are not canonically conjugate.

Both problems can be solved simultaneously by using a Hamiltonian description for field lines and a convenient coordinate system. The latter should provide naturally the toroidicity effect, such as the so-called toroidal polar coordinates (r_t,θ_t,φ), as described in Ref. [38]. The coordinate surfaces are tori whose axes are displaced from the magnetic axis (located at R'_0, which is slightly different from the major radius R_0), so emulating the Shafranov shift of magnetic surfaces. In the large aspect ratio approximation the toroidal polar coordinates reduce to the local coordinates used in the UM.

From the toroidal polar coordinate one can define canonically conjugate action-angle variables as [39]

$$J(r_t) = \frac{1}{4}\left[1 - \sqrt{1 - 4\left(\frac{r_t}{R'_0}\right)^2}\right], \tag{11}$$

$$\vartheta(r_t,\theta_t) = 2\arctan\left[\frac{1}{\Omega(r_t)}\left(\frac{\sin\theta_t}{1+\cos\theta_t}\right)\right], \tag{12}$$

where

$$\Omega(r_t) = \sqrt{\frac{1-2r_t/R'_0}{1+2r_t/R'_0}}. \tag{13}$$

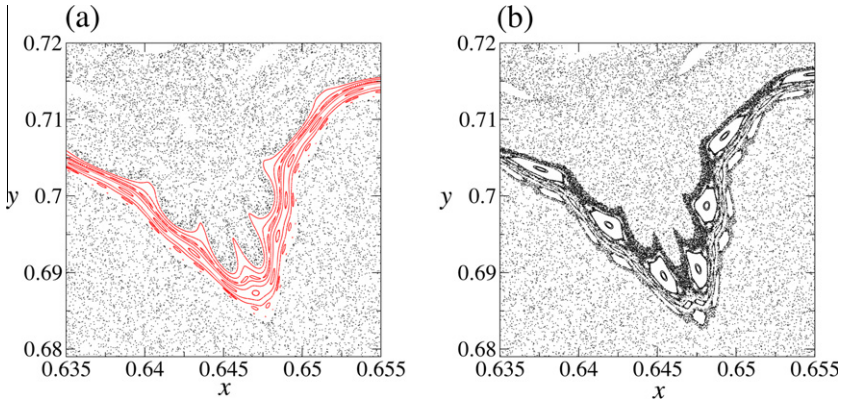

Fig. 4. Magnification of a region of a phase portraits for UM for (a) $\epsilon = 0.3029$, and (b) $\epsilon = 0.3031$.

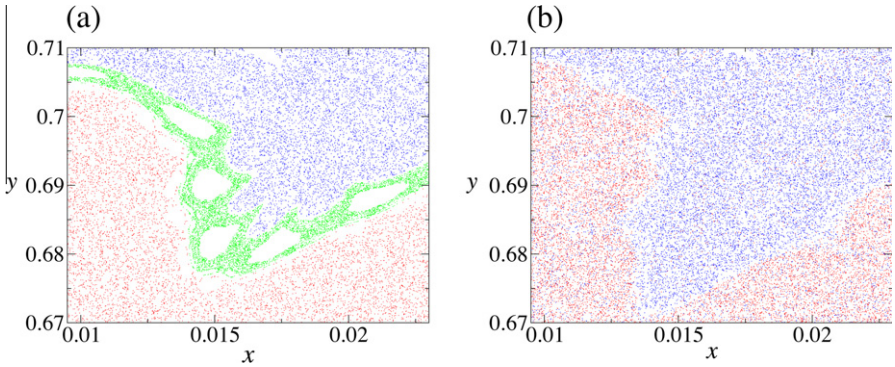

Fig. 5. Magnification of a region of a phase portraits for UM (a) $\epsilon = 0.3031$, and (b) $\epsilon = 0.3040$.

On considering the field line Hamiltonian in terms of these action and angle variables, we expand the unperturbed Hamiltonian around a given magnetic surface with action $J = J_0$ and a rational winding number $\Omega_0 = n/m$, where n and m are two integers. Nontwist maps arise from non-monotonic radial profiles for the winding number, such as

$$H_0(\Delta J) = \frac{1}{2}(\Delta J)^2 - \frac{\alpha}{3}(\Delta J)^3, \tag{14}$$

where $\Delta J = J - J_0$ and $\alpha = H_0'(J_0)/2H_0''(J_0)$, such that the winding number is $\Omega_0 = dH_0/d(\Delta J)$ [40–42].

We are interested, like in the UM, to describe the perturbation of a magnetic ergodic limiter on the integrable Hamiltonian described above. The two dominant resonant modes excited by such a perturbation have poloidal wave numbers equal to m and $m + 1$, respectively, representing the main resonant island and its bigger satellite island. The interaction between these two island chains reproduces quite well the transition to field line chaos.

While the UM assumes the existence of only one ergodic limiter at a fixed position $\varphi = 0$, we can describe an arbitrary number N_r of limiters, each of them located at toroidal positions $n(2\pi/N_r)$, where $n = 0, 1, 2, \ldots, N_r - 1$. We consider the map of a field line from the k-th surface of section to the following one as

$$(\Delta J)_{k+1} = (\Delta J)_k + m\beta \sin(m\vartheta_{k+1}) + (m+1)\eta \sin((m+1)\vartheta_{k+1} + nt_{k+1}), \tag{15}$$

$$\vartheta_{k+1} = \vartheta_k + \frac{2\pi}{N_r}((\Delta J)_k - \alpha(\Delta J)_k^2), \quad (\mathrm{mod}\ 2\pi), \tag{16}$$

$$t_{k+1} = t_k + \frac{2\pi}{mN_r}, \tag{17}$$

which, despite being described by three equations, is still a two-dimensional symplectic map [41,42].

In Fig. 6(a) we show a phase portrait of the two-mode map (15)–(17) which illustrates a non-twist equilibrium field line structure with two isochronous resonances with winding number 1/3. The latter have already reconnected and dimerized, being separated by a set of meandering invariant curves. Such curves encircle both sets of island chains and can appear only

for nontwist maps near the shearless curve. Fig. 6(b) shows that the region near the shearless curve acts as an internal transport barrier separating two chaotic areas and avoiding the radial diffusion.

Although the exact numerical integration of the magnetic field line equation yields Poincaré maps that reflect in a rather precise way the nontwist dynamics, this procedure is a very time-consuming computational task. Many studies of long-term behavior of this system, as analyzes of diffusion, escape or loss of field lines, require a computationally fast and reliable scheme of numerical integration. Instead of obtaining numerically the Poincaré maps, we can resort to the impulsive nature of the ergodic limiter to obtain a local analytical approximation of the exact mapping.

Comparing the numerical results obtained with the maps of Sections 3 and 4 we recognize that, taking only one resonant term may be not enough, for some equilibrium parameters, to form inside the tokamak plasma the large chaotic region numerically obtained even for large amplitude perturbations. Hence, in the two-mode map we also take into account a second resonant mode from the infinite number of Fourier harmonics generated by the ergodic limiter. Consideration of additional resonances would improve our description of the chaotic region, but they are not necessary to study the transport barrier in the shearless region where the two considered modes are dominant.

4. Drift wave maps

Experiments indicate that in tokamaks the plasma confinement depends on the anomalous particle transport at the plasma edge caused by the electrostatic turbulence [43]. Thus it is important to estimate the contribution to this transport due to the chaotic particle orbits driven by the turbulent fluctuation. The transport of particles in a magnetically confined plasma, due to electrostatic drift waves, has been investigated [18]. The model describes the trajectory of the guiding center of a plasma particle in a uniform magnetic field perpendicular to a radial electric field perturbed by drift waves, using the Hamiltonian description for the guiding center trajectory [43].

The $\mathbf{E}\times\mathbf{B}$-drift produced by the equilibrium radial electric field and a dominant wave is described by the integrable part of the Hamiltonian, while the other part contains the perturbation representing the fluctuating electric field associated to other drift waves. Within this framework the Lagrangian chaotic transport of the guiding centers of ions is calculated and proposed to interpret the anomalous plasma edge transport observed in tokamaks [18]. Resonances and island chains created at the plasma edge depend on the main plasma parameters and the radial electric field and plasma flow radial profiles [20]. We use the chaotic orbits to determine the particle radial transport.

In the model considered in this work, single particle motion in the equilibrium plasma is described by an integrable Hamiltonian system and can be solved analytically. However for the plasma perturbed by a set of coherent drift waves the Hamiltonian is no longer integrable. Thus, qualitative features of this transport can be approximated by a low-dimensional dynamical system with island chains in phase space due to the superposition of many dominant waves.

The drift velocity of the guiding centers is given by:

$$\mathbf{v} = -\frac{\nabla\phi\times\mathbf{B}}{B^2}, \tag{18}$$

which is equivalent to the following set of differential equations:

$$v_x = \frac{dx}{dt} = -\frac{1}{B_0}\frac{\partial\phi}{\partial y}, \tag{19}$$

$$v_y = \frac{dy}{dt} = \frac{1}{B_0}\frac{\partial\phi}{\partial x}, \tag{20}$$

representing canonical equations obtained from a drift-wave Hamiltonian $H(x,y,t) = \phi(x,y,t)/B_0$. The electric potential is given by

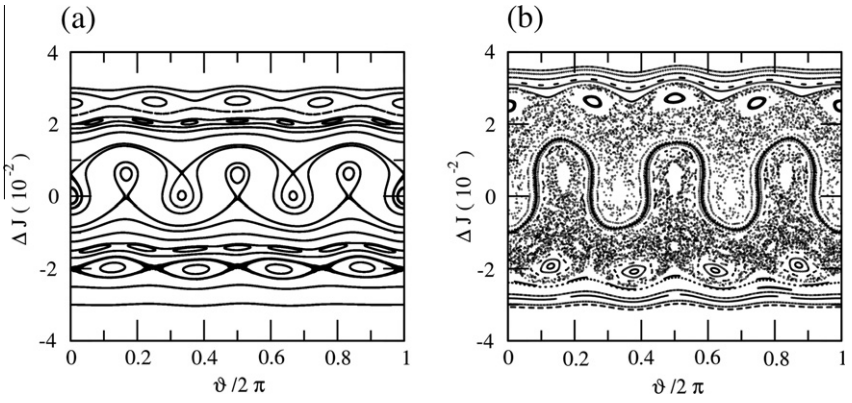

Fig. 6. Phase portraits for the two-mode map with $m = 3$, $\alpha = 160.15$, (a) $\beta = -4.96\times10^{-5}$, $\eta = 2.29\times10^{-5}$ and (b) $\beta = -1.30\times10^{-4}$, $\eta = 1.15\times10^{-4}$.

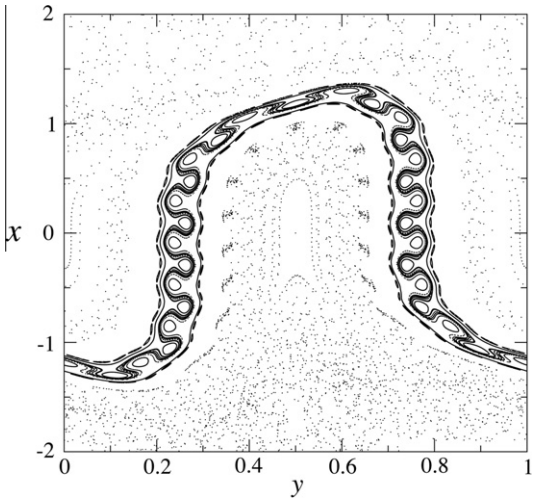

Fig. 7. Phase portrait for the nontwist drift wave map (23) and (24) with $a_1 = 0.384$ and $b_1 = 0.1$.

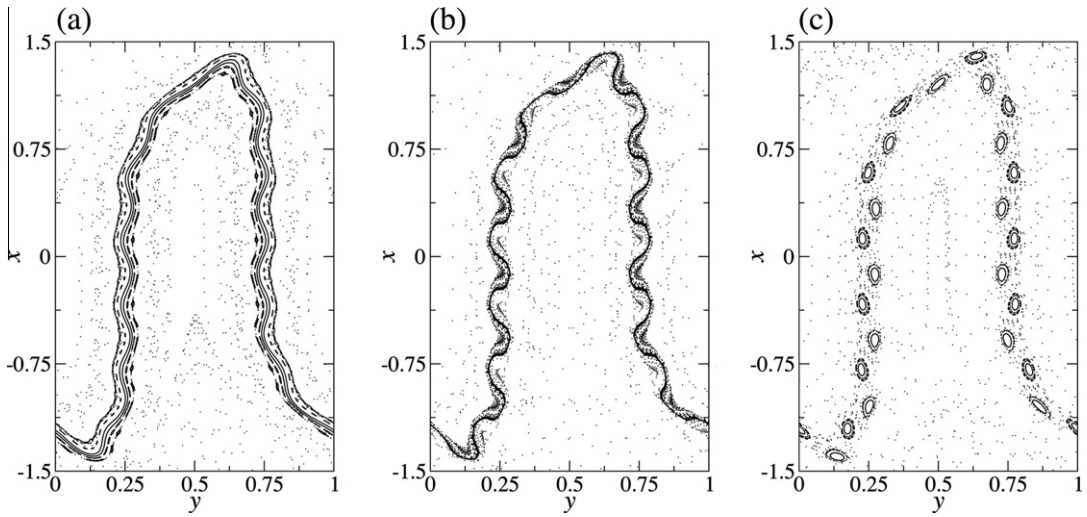

Fig. 8. Phase portrait for the nontwist drift wave map (23) and (24) with $b_1 = 0.1$ and (a) $a_1 = 0.455$; (b) $a_1 = 0.460$; (c) $a_1 = 0.464$.

$$\phi(x,y,t) = \phi_0(x) + \sum_{j=-\infty}^{+\infty} A\cos(k_y y - j\omega_0 t). \tag{21}$$

We can choose a non-monotonic x-profile for the equilibrium electric potential $\phi(x)$ and integrate Eq. (21) to obtain a nontwist drift map.

In this work we introduce a nontwist map that could be used to simulate local transport barriers observed at the plasma edge. For that, we identify an observed radial transport barrier as resulting from a nontwist map that locally describes the particle trajectories around the transport barrier. To obtain such map, we choose an equilibrium electric potential that gives a proper nonmonotonic electric field corresponding to a nonmonotonic flow simulating a localized transport barrier in the nontwist region. This local nontwist property would be created by an instability or a local flow at the plasma edge that locally taylors the electric field radial profile. A convenient potential for that is

$$\phi_0 = \begin{cases} -\alpha x^4 & \text{if } x < 0, \\ \alpha x^4 & \text{if } x \geqslant 0. \end{cases} \tag{22}$$

for which we obtain a nontwist drift wave map, given by

$$x_{n+1} = x_n + a_1 \sin(2\pi y_n), \tag{23}$$

$$y_{n+1} = y_n + b_1 |x_{i+1}|^3, \quad (\text{mod } 1), \tag{24}$$

where the parameters a_1 and b_1 are determined from the equilibrium and perturbing quantities.

Fig. 7 shows a representative phase portrait of the dynamics generated by this nontwist drift wave map. For the parameters chosen we observe the formation of an internal transport barrier between two regions almost completely chaotized. This barrier, on its hand, has been formed thanks to the meandering curves appearing near the shearless curve in a reconnection process very similar to that described in the previous section for a field line map. Inside the transport barrier shown in Fig. 7 we identify invariant curves and island chains embedded on it. These chains with a large number of dimerized islands appear on both sides of the invariant curves (in fact, one of these invariant curves is a shearless curve).

In Fig. 8(a)–(c) we can recognize the barrier breakup process observed by keeping a constant b_1-value and changing the parameter a_1 from 0.455 to 0.464. On increasing the control parameter a_1, the barrier becomes thinner and changes until it breaks up in a scenario of successive bifurcations that gives rise to a sequence of new island chains. After the barrier breakup two dimerized island chains survive further for a small parameter a_1-variation.

The drift map may be useful to investigate the sudden onset of a plasma edge transport barrier. This is a local alteration in the plasma in contrast with the barrier created by magnetic resonances whose modes have a global influence on the Poincaré surfaces described by the maps of Sections 2 and 3.

5. Conclusions

Nontwist symplectic maps have been intensively studied in the past years due to their intrinsic mathematical appeal (KAM theorem, for example, does not hold for them) as well as their occurrence in many problems of physical interest, particularly in plasma physics. In this work we reviewed nontwist symplectic maps that we have introduced to describe chaotic Lagrangian transport in plasmas confined in tokamaks. The presented maps are derived from plasma models with non-monotonic equilibrium field profiles and control parameters that are commonly measured in plasma discharges. Moreover, these analytical maps can be used to investigate long-term transport properties, by replacing lengthy numerical integrations of the magnetic field line equations by faster map iterations.

The maps describe two kinds of transport at the plasma edge, namely, the escape of chaotic magnetic field lines from the plasma to the wall, as well as the chaotic anomalous particle transport due to the $\mathbf{E} \times \mathbf{B}$ drift motion associated to the electrostatic fluctuations. Initially, we presented two maps that we have used to describe barriers that obstruct or reduce the magnetic field line transport due to resonant perturbations at the plasma edge created by an ergodic limiter. After that, we present a new map that describes the particle drift transport associated to the electrostatic drift waves.

In all maps we presented in this work, we focused on the formation and destruction of transport barriers in the shearless region. Such transport barriers are desirable in tokamaks because they reduce particle losses and improve plasma confinement. The barriers were found to be very robust, demanding strong perturbations to destroy them. Furthermore we described how an effective barrier reduces the transport across the shearless region. This behavior is caused by the higher order island chains present in the shearless region, due to the non-monotonicity of the equilibrium field profiles. The main transport properties observed in the nontwist tokamak maps are common to those observed in the standard nontwist map, some of them having been analytically predicted in the literature, especially in the papers of Phil Morrison and his collaborators.

Acknowledgments

This work was made possible by partial financial support of FAPESP, CNPq, CAPES, MCT/CNEN (Rede Nacional de Fusão) and Fundação Araucária (State of Paraná).

References

[1] Lichtenberg AN, Lieberman MA. Regular and chaotic dynamics. 2nd ed. Berlin: Springer-Verlag; 1992.
[2] Meiss JD. Symplectic maps, variational principles, and transport. Rev Mod Phys 1992;64:795–848.
[3] Abdullaev SS. Construction of mappings for Hamiltonian systems and their applications. Lecture notes in physics, vol. 691. Berlin: Springer-Verlag; 2006.
[4] Morrison PJ. Magnetic field lines, Hamiltonian dynamics, and nontwist systems. Phys Plasmas 2000;7:2279–89.
[5] Petrisor E. Nontwist area-preserving maps with reversing symmetry group. Int J Bifur Chaos 2001;11:497–511.
[6] Delshams A, de la Llave R. KAM theory and a partial justification of Greene's criterion for nontwist maps. SIAM J Math Anal 2000;31:1235–69.
[7] Franks J, LeCalvez P. Regions of instability for non-twist maps. Ergod Therm Dyn Sys 2003;23:111–41.
[8] Simó C. Invariant curves of analytic perturbed nontwist area preserving maps. Reg Chaotic Dyn 1998;3:180–95.
[9] Dullin HR, Meiss JD, Sterling D. Generic twistless bifurcations. Nonlinearity 2000;13:203.
[10] del-Castillo-Negrete D, Morrison PJ. Magnetic field line stochasticity and reconnection in a non-monotonic q-profile. Bull Am Phys Soc Ser II 1992;37:1543.
[11] Kroetz T, Marcus FA, Roberto M, Caldas IL, Viana RL. Transport control in fusion plasmas by changing electric and magnetic field spatial profiles. Comput Phys Commun 2009;180:642–50.
[12] Kerner W, Tasso H. Stability of multihelical tearing modes in shaped tokamaks. Phys Rev Lett 1982;49:654.
[13] Davidson MG, Dewar RL, Gardner HJ, Howard J. Hamiltonian maps for Heliac magnetic islands. Aust J Phys 1995;48:871.
[14] Wingen A, Jakubowski M, Spatschek KH, Abdullaev SS, Finken KH, Lehnen A. Traces of stable and unstable manifolds in heat flux patterns. Phys Plasmas 2007;14:042502.
[15] Pierrehumbert RT. Largescale horizontal mixing in planetary atmospheres. Phys Fluids A 1991;3:1250–60.

[16] del-Castillo-Negrete D, Morrison PJ. Hamiltonian chaos and transport in quasigeostrophic flows. In: Prigogine I, editor. Chaotic dynamics and transport in fluids and plasmas. New York: American Institute of Physics; 1992. p. 181207.
[17] del-Castillo-Negrete D, Morrison PJ. Chaotic transport by Rossby waves in shear flow. Phys Fluids A 1993;5:948965.
[18] Horton W, Park HB, Kwon JM, Strozzi D, Morrison PJ, Choi DI. Drift wave test particle transport in reversed shear profile. Phys Plasmas 1998;5:39103917.
[19] del-Castillo-Negrete D. Chaotic transport in zonal flows in analogous geophysical and plasma systems. Phys Plasmas 2000;7:17021711.
[20] Marcus AF, Caldas IL, Guimarães-Filho ZO, Morrison PJ, Horton W, Nascimento IC, et al. Reduction of chaotic particle transport driven by drift waves in sheared flow. Phys Plasmas 2008;15:112304.
[21] Oda GA, Caldas IL. Dimerized island chains in tokamaks. Chaos Soliton Fractals 1995;5:15–23.
[22] de Carvalho RE, de Almeida AMO. Integrable approximation to the overlap of resonances. Phys Lett A 1992;162:457–63.
[23] Chandre C, Farrelly DF, Uzer T. Thresholds to chaos and ionization for the hydrogen atom in rotating fields. Phys Rev A 2002;65:053402.
[24] Portela JSE, Caldas IL, Viana RL, Morrison PJ. Diffusive transport through a nontwist barrier in tokamaks. Int J Bifurcat Chaos 2007;17:1589–98.
[25] Morrison PJ, Wurm A. Nontwist maps. Scholarpedia 2009;4(9):3551. <http://www.scholarpedia.org/article/Nontwist_maps>.
[26] Szezech Jr JD, Caldas IL, Lopes SR, Viana RL, Morrison PJ. Transport properties in nontwist area-preserving maps. Chaos 2009;19:043108.
[27] Wurm A, Apte A, Morrison PJ. On reconnection phenomena in the standard nontwist map. Braz J Phys 2004;34:1700–6.
[28] Wurm A, Apte A, Fuchss K, Morrison PJ. Separatrix reconnection, and meanders in the standard nontwist map. Chaos 2005;15:023108.
[29] Hazeltine RD, Meiss JD. Plasma confinement. Dover; 2003.
[30] Connor JW, Fukuda T, Garbet X, Gormezano C, Mukhovatov V, Wakatani M, et al. the ITB database group, the ITPA topical group on transport and internal barrier physics. A review of internal transport barrier physics for steady-state operation of tokamaks. Nucl Fusion 2004;44:R1–R49.
[31] Evans TE, Goniche M, Grosman A, Guilhem D, Hess W, Vallet J-C. Magnetic perturbation effects on boundary plasmas during high power lower hybrid current drive in Tore Supra. J Nucl Mat 1992;196(198):421–5.
[32] Jakubowski MW, Abdullaev SS, Finken KH. the TEXTOR Team, modelling of the magnetic field structures and first measurements of heat fluxes for TEXTOR-DED operation. Nucl Fusion 2004;44:S1–S11.
[33] Karger F, Lackner F. Resonant helical divertor. Phys Lett A 1975;61:385–7.
[34] Ghendrih Ph, Bécoulet M, Colas L, Grosman A, Guirlet R, Gunn J, et al. Tore Supra team, progress in ergodic divertor operation on Tore Supra. Nucl Fusion 2002;42:1221–50.
[35] Caldas IL, Viana RL, Vannucci A, da Silva EC, Araujo MST, Ullmann K, et al. Control of chaotic magnetic fields in Tokamaks. Braz J Phys 2002;32.
[36] Balescu R, Vlad M, Spineanu F. Tokamap: a Hamiltonian twist map for magnetic field lines in a toroidal geometry. Phys Rev E 1998;58:951–64.
[37] Ullmann K, Caldas IL. A symplectic mapping for the ergodic magnetic limiter an its dynamical analysis. Chaos Soliton Fractals 2000;11:2129–40.
[38] Kucinski MY, Caldas IL. Resonant helical fields. Z Naturforsch 1987;42:1124.
[39] da Silva EC, Caldas IL, Viana RL. Field line diffusion and loss in a Tokamak with an ergodic magnetic limiter. Phys Plasmas 2001;8:2855–65.
[40] Kroetz T, Roberto M, da Silva EC, Caldas IL, Viana RL. Escape patterns of chaotic magnetic field lines in a tokamak with reversed magnetic shear and an ergodic limiter. Phys Plasmas 2008;15:092310–1/12.
[41] Roberto M, da Silva EC, Caldas IL, Viana RL. Derivation of an analytical area-preserving map to describe transport barriers in tokamaks. J Phys E (Conf Ser) 2005;7:163–73.
[42] Roberto M, da Silva EC, Caldas IL, Viana RL. Transport barrier created by dimerized islands. Phys A 2004;342:363–9.
[43] Horton W. Drift waves and transport. Rev Mod Phys 1999;71:735–78.